

# Synthesis and characterization of precursor derived TiN@Si-Al-C-N ceramic nanocomposites for oxygen reduction reaction

Eranezhuth Wasan Awin<sup>1</sup> | Timon E. Günther<sup>2</sup>  | Rameshwori Loukrakpam<sup>2</sup> |  
Stefan Schafföner<sup>1</sup>  | Christina Roth<sup>2</sup> | Günter Motz<sup>1</sup> 

<sup>1</sup>Department of Ceramic Materials Engineering, University of Bayreuth, Bayreuth, Germany

<sup>2</sup>Department of Electrochemical Process Engineering, University of Bayreuth, Bayreuth, Germany

## Correspondence

Günter Motz, Department of Ceramic Materials Engineering, University of Bayreuth, Prof.-Rüdiger Bormann-Str. 1, 95447 Bayreuth, Germany.

Email: [guenter.motz@uni-bayreuth.de](mailto:guenter.motz@uni-bayreuth.de)

## Funding information

Deutsche Forschungsgemeinschaft; Agence Nationale de la Recherche

## Abstract

The development of efficient and durable catalysts is critical for the commercialization of fuel cells, as the catalysts' durability and reactivity dictate their ultimate lifetime and activity. In this work, amorphous silicon-based ceramics (Si-C-N and Si-Al-C-N) and TiN@Si-Al-C-N nanocomposites were developed using a precursor derived ceramics approach. In TiN@Si-Al-C-N nanocomposites, TiN nanocrystals (with sizes in the range of 5–12 nm) were effectively anchored on an amorphous Si-Al-C-N support. The nanocomposites were found to be mesoporous in nature and exhibited a surface area as high as 132 m<sup>2</sup>/g. The average pore size of the nanocomposites was found to increase with an increase in the pyrolysis temperature, and a subsequent graphitization of free carbon was observed as revealed from the Raman spectra. The ceramics were investigated for electrocatalytic activity toward the oxygen reduction reaction using the rotating disk electrode method. The TiN@Si-Al-C-N nanocomposites showed an onset potential of 0.7 V versus reversible hydrogen electrode for oxygen reduction, which seems to indicate a 4-electron pathway at the pyrolysis temperature of 1000°C in contrast to a 2-electron pathway exhibited by the nanocomposites pyrolyzed at 750°C via the Koutecky–Levich plot.

## KEY WORDS

catalysts/catalysis, characterization, nanocomposites, polymer precursor, silicon carbonitride

## 1 | INTRODUCTION

The global energy demand and environmental pollution drive the need for continuous improvement of existing sustainable energy devices. Out of which, electrocatalytic devices (e.g., fuel cells) have raised considerable interest due to their high energy density and power density.<sup>1,2</sup> The oxygen reduction reaction (ORR) is very important

in electrocatalysis, and platinum-based electrocatalysts have been proven to be among the best in terms of their performance.<sup>3</sup> Currently, platinum on a carbon support is the most extensively used ORR catalyst. However, the use of noble metals increases the overall cost of the electrocatalytic devices. Furthermore, platinum-based electrocatalysts are also known to be not long-term stable under fuel cell working conditions.<sup>4,5</sup> Under these

This is an open access article under the terms of the [Creative Commons Attribution](https://creativecommons.org/licenses/by/4.0/) License, which permits use, distribution and reproduction in any medium, provided the original work is properly cited.

© 2022 The Authors. *International Journal of Applied Ceramic Technology* published by Wiley Periodicals LLC on behalf of American Ceramics Society.

3 circumstances, the need for alternative low-cost, robust,  
4 and stable electrocatalysts is substantial.

5 Owing to the high electrical conductivity, nitrogen-  
6 doped carbon materials and transition metal nitrides  
7 have been tested in previous projects and reported to  
8 exhibit promising ORR activity.<sup>6-9</sup> Herein, the pres-  
9 ence of nitrogen is believed to raise the conduction  
10 band and thus increase the ORR activity.<sup>10,11</sup> There have  
11 been several studies using porous nitrogen-doped carbon  
12 materials as favorable electrocatalytic supports.<sup>12-14</sup> This  
13 includes nitrogen-doped carbon nanotubes/graphene,<sup>15</sup>  
14 carbon spheres,<sup>16</sup> carbon fibers,<sup>17</sup> and graphitic-C<sub>3</sub>N<sub>4</sub>.<sup>18</sup>  
15 Liu et al. reported an Si-C material in which bonding  
16 silicon to carbon was shown to excite electrons more  
17 readily to oxygen when compared to pristine graphene.<sup>19</sup>  
18 Furthermore, the electrochemical activity of transition  
19 metal nitrides on carbon supports was investigated, and  
20 high onset potentials and ORR current densities were  
21 observed.<sup>20,21</sup> Even though the aforementioned material  
22 systems exhibited significant ORR activity, the practical  
23 use of these materials is still restricted due to their poor  
24 corrosion resistance and scalability issues.<sup>22,23</sup>

25 In this context, silicon carbonitride (silicon-based pre-  
26 cursor derived ceramics [PDC], Si-C-N), known for its  
27 excellent stability, chemical resistance, and ease in process-  
28 ability, could be a viable candidate for electrocatalysts. The  
29 presence of free carbon in the system could be a determin-  
30 ing factor in enhancing the catalytic properties. The tech-  
31 nical possibilities that PDCs have to offer, in particular, tai-  
32 loring the ceramics properties at the molecular scale, make  
33 the approach appreciable for functional applications.<sup>24-27</sup>  
34 For instance, the addition of aluminum into the back-  
35 bone of the Si-C-N network could enhance the electrical  
36 conductivity and is thereby believed to improve the elec-  
37 trocatalytic activity.<sup>28</sup> The functional properties could also  
38 be tuned by incorporating transition metal oxides, nitrides,  
39 and carbides into the structure. Hence, in this study, amor-  
40 phous Si-C-N and silicon aluminum carbonitride (Si-Al-  
41 C-N) ceramics were synthesized using a PDC approach.  
42 In addition, a combinatorial technique that involves PDC  
43 with urea-glass route was used to produce TiN@Si-Al-  
44 C-N nanocomposites. The aforementioned materials were  
45 evaluated for their ORR activity.

## 47 2 | EXPERIMENTAL METHODS

### 50 51 2.1 | Synthesis of porous Si-C-N and 52 Si-Al-C-N supports

53 In an attempt to synthesize porous Si-C-N, hydroxy-  
54 terminated polyethylene (PEOH) dissolved in toluene was  
55 made to react with polysilazane (Durazane 1800, Merck

KGaA, Germany) in 70:30 by weight at 110°C under static conditions for 1 h to synthesize a block copolymer (HTT1800-b-PE). Because of its high crystallinity and reactive hydroxyl end group, the inexpensive PEOH was chosen as a latent pore former block and to connect with the HTT1800 block. To produce porous Si-Al-C-N ceramics, aluminum acetylacetone (dissolved in toluene) was added to the aforementioned mixture in 90:10 weight ratio, and subsequently, cross-linking was commenced by the addition of dicumyl peroxide. The temperature of the preceramic polymeric mixture was maintained for 12 h and then cooled to room temperature. The solvent was then removed, and the resulting precursor was transferred to the tube furnace. The polymeric precursor was then pyrolyzed at 800°C in nitrogen atmosphere for half an hour to obtain porous Si-Al-C-N ceramics. During the heating cycle, heating rate was maintained at 1°C/min up to 300°C and then 5°C/min up to 800°C. Throughout the pyrolysis, the material was held at 300, 400, and 500°C for 2 h in nitrogen atmosphere.

### 2.2 | Synthesis of TiN nanocrystals anchored on porous Si-Al-C-N ceramic supports

TiN nanocrystals anchored on porous Si-Al-C-N ceramic supports were prepared using TiCl<sub>4</sub> (Merck KGaA, Germany) as a TiN precursor. In a typical synthesis procedure, 2.5 ml of ethanol was added to 1 g of TiCl<sub>4</sub> to which 1583 mg of urea (molar ratio of urea to TiCl<sub>4</sub> was maintained to be five) and 100 mg of Si-Al-C-N in 15 ml of ethanol were added subsequently. The mixture was stirred for 1 h, and the solution was kept at 100°C overnight to remove the solvent. The viscous mixture was then pyrolyzed at two different temperatures (750 and 1000°C) maintaining a heating rate of 3°C/min and held for 3 h in nitrogen atmosphere, which hereafter will be referred to as TiN@Si-Al-C-N\_750 and TiN@Si-Al-C-N\_1000.

### 2.3 | Materials characterization

The bonding characteristics were analyzed from Fourier transform infrared (FTIR) analysis (Bruker Tensor 27, USA). Raman spectroscopy was carried out using a Bruker SENTERRA II, USA confocal microscope with a 532 nm excitation laser to analyze the presence of free carbon. The crystalline nature of the prepared catalysts was evaluated by X-ray diffraction (XRD, D8 ADVANCE Bruker AXS, Germany). The micro/nanostructural characteristics were visualized using scanning electron microscopy (SEM,

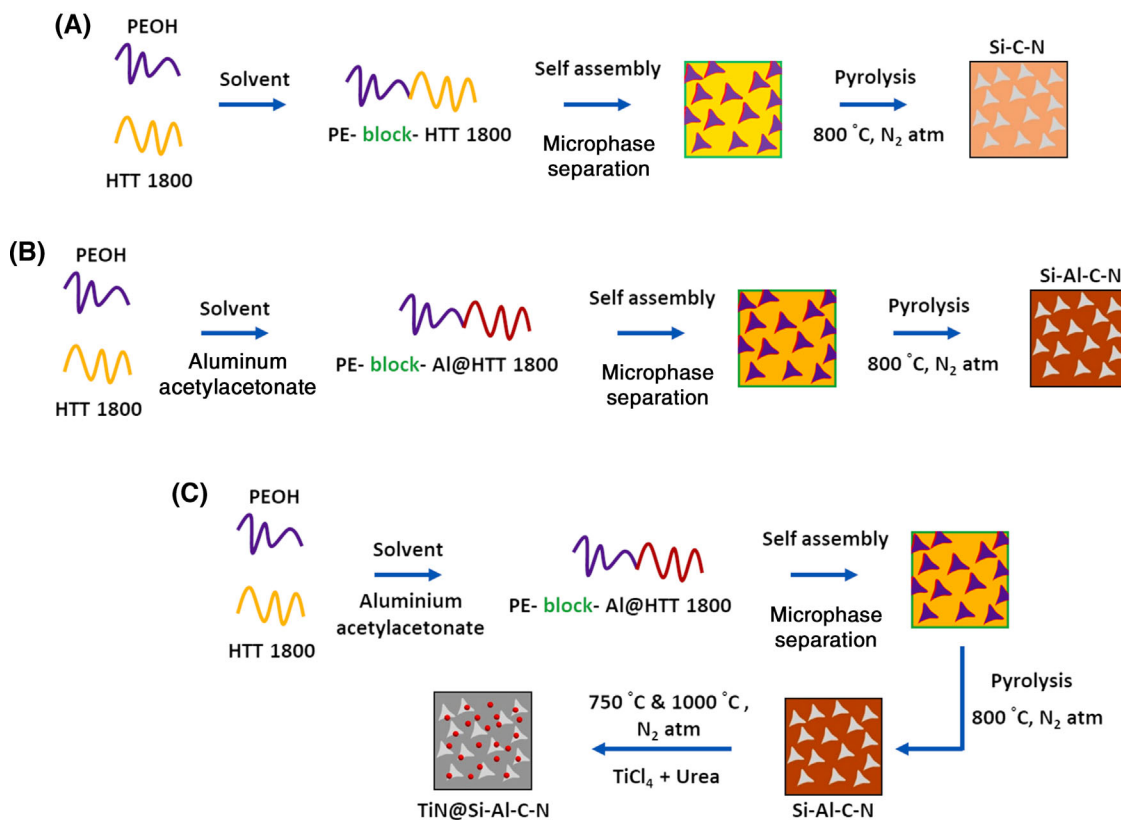


**FIGURE 1** Generalized scheme for the synthesis of (A) Si-C-N ceramics, (B) Si-Al-C-N ceramics, and (C) TiN@Si-Al-C-N nanocomposites

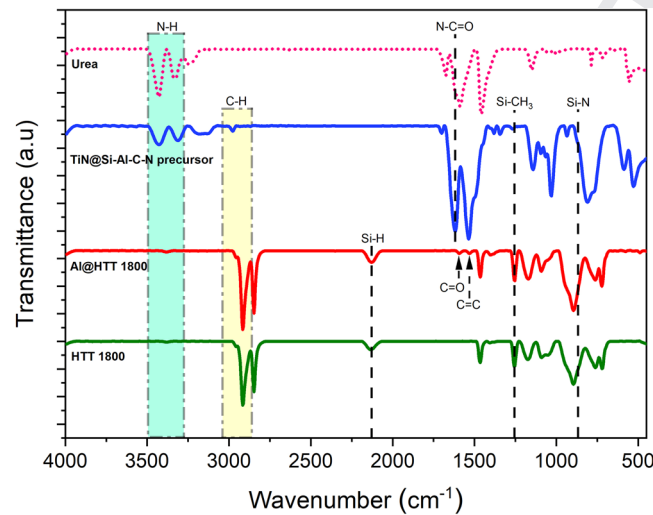


**FIGURE 2** Fourier transform infrared (FTIR) spectra of HTT 1800, aluminum modified HTT 1800, and metal nitride precursors prepared using two different strategies

Gemini Sigma 300 VP, Carl Zeiss AG, Germany) and transmission electron microscopy (TEM) (JEOL JEM-2200FS, 200 kV, Germany). The porosity of the catalysts was determined using BET analysis (Nova 2000e, Quantachrome, USA).

## 2.4 | Electrochemical measurements

The evaluation of the ORR activity of the prepared silicon-based ceramics and the nanocomposites (hereafter referred to as catalysts) was performed using an electrochemical setup with Bio-Logic VSP 300 potentiostat and a Pine Research rotator controller. A standard electrochemical glass cell with a volume of 100 ml was used for the electrochemical performance tests. A three-electrode setup with a reversible hydrogen electrode (RHE, HydroFlex from Gaskatel) as reference electrode, platinum coil as counter electrode, and glassy carbon electrode RDE tip ( $\phi = 5$  mm) with a catalyst layer as the working electrode was employed in 1 M KOH electrolyte and kept at 25°C. The glassy carbon RDE tip was first polished with alumina particles of (average) size .3 and .05  $\mu$ m in suspension (from Buehler) and rinsed with ultrapure water (Milli-Q, 18.2 M $\Omega$  cm). The preparation of the catalyst layer is as follows: 10 mg of the catalyst powder was taken, and 2.5 ml ultrapure water and 2.5 ml isopropanol were added, then 50  $\mu$ l of 10 wt% Nafion solution (from Alfa Aesar) was added to it. The glass vial containing the mixture was placed in an ultrasonic bath filled with cold water (<5°C) and sonicated (37 kHz, 100% Power, Elmasonic P) for 15 min. For preparing the catalyst film, a volume of

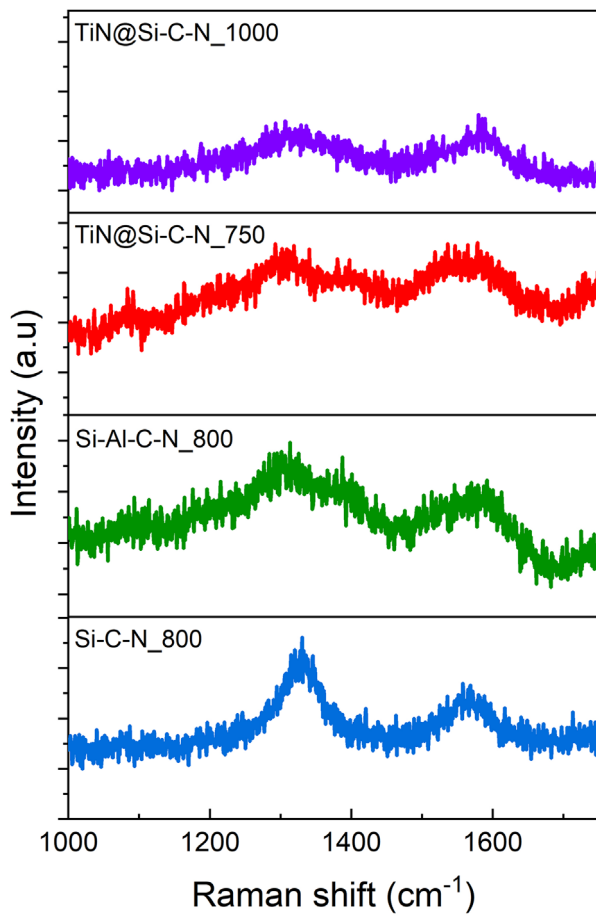


FIGURE 3 Raman spectra of synthesized silicon-based ceramics indicating the presence of free carbon by the characteristic D and G band

50  $\mu$ l was dropped in several steps on the cleaned and polished glassy carbon electrode (geometrical surface area .196  $\text{cm}^2$ ) that was dried during rotation at 700 rpm under ambient conditions. Pretreatment steps in electrolyte saturated with  $\text{N}_2$  and  $\text{O}_2$  were done on the RDE tips with a catalyst layer using cyclic voltammograms (CVs) in a potential range of +1.1 to +1.0 V versus RHE with a scan rate of 200 mV/s (50 cycles each) to activate the surface of the catalysts. Open circuit voltage (OCV) was held for 30 min with gas bubbling before recording the CVs. The ohmic drop was compensated at 85% using a positive feedback method, which left an uncompensated resistance of  $\sim 5 \Omega$  or less in the electrochemical cell. RDE measurements were carried out at the rotating speeds of 100, 400, 900, 1600, and 2200 rpm using linear sweep voltammetry (LSV) to record the current densities ( $\text{mA}/\text{cm}^2$  of the geometrical surface area) in saturated  $\text{O}_2$  in the potential range of .05–1.2 V with 20 mV/s scan rate. Three cycles were recorded for each rotating speed, and the third cycle was used for analysis. Additionally, the  $\text{N}_2$  background current was collected for the same potential range and

TABLE 1 Variation of  $I_D/I_G$  ratio of Si-C-N ceramics with the modification of Al and TiN

Samples	$I_D/I_G$
Si-C-N	1.91
Si-Al-C-N	1.60
TiN@Si-Al-C-N_750	1.13
TiN@Si-Al-C-N_1000	.93

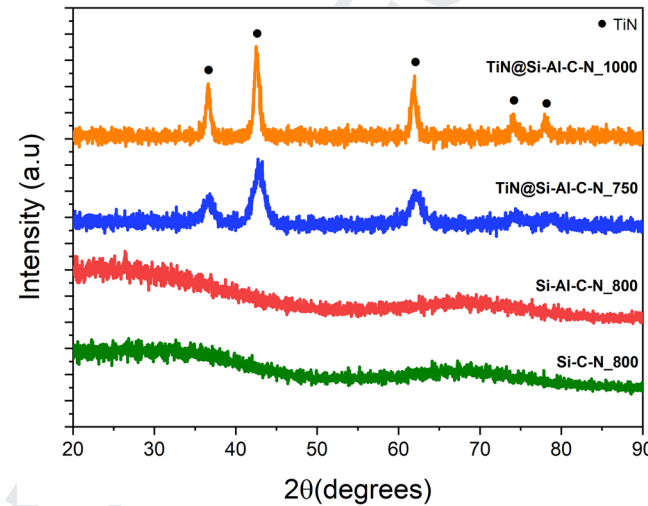


FIGURE 4 X-ray diffractograms of synthesized silicon-based ceramics revealing the amorphous nature of the substrates and crystallization of titanium nitride after pyrolysis

scan rate at 1600 rpm and subtracted from the ORR current densities to eliminate any capacitive current. Reported results are based on kinetic parameters of the Koutecky-Levich equations. An additional CV was performed with 5 mV/s scan rate in  $\text{O}_2$  saturated electrolyte with no rotation. OCV was held for 15 min to saturate the electrolyte with  $\text{O}_2$  before chrono-amperometric (CA) measurements on TiN@Si-Al-C-N\_1000 at the potential of .6 V for 2 h. The ORR activity was recorded for TiN@Si-Al-C-N\_1000, in  $\text{O}_2$ -saturated .1 M KOH solution with a slow scan rate of 5 mV/s and a rotation rate of 1600 rpm before and after the CA.

### 3 | RESULTS AND DISCUSSION

Figure 1 represents the generalized scheme of reactions used to synthesize Si-C-N, Si-Al-C-N and TiN@Si-Al-C-N ceramics. The first stage involves the synthesis of Si-C-N ceramics by reacting HTT 1800 with PEOH. This led to the formation of PE-block-HTT1800 by self-assembly that upon pyrolysis in nitrogen atmosphere decomposes to form amorphous and porous Si-C-N. In order to synthesize aluminum modified Si-C-N ceramics, aluminum

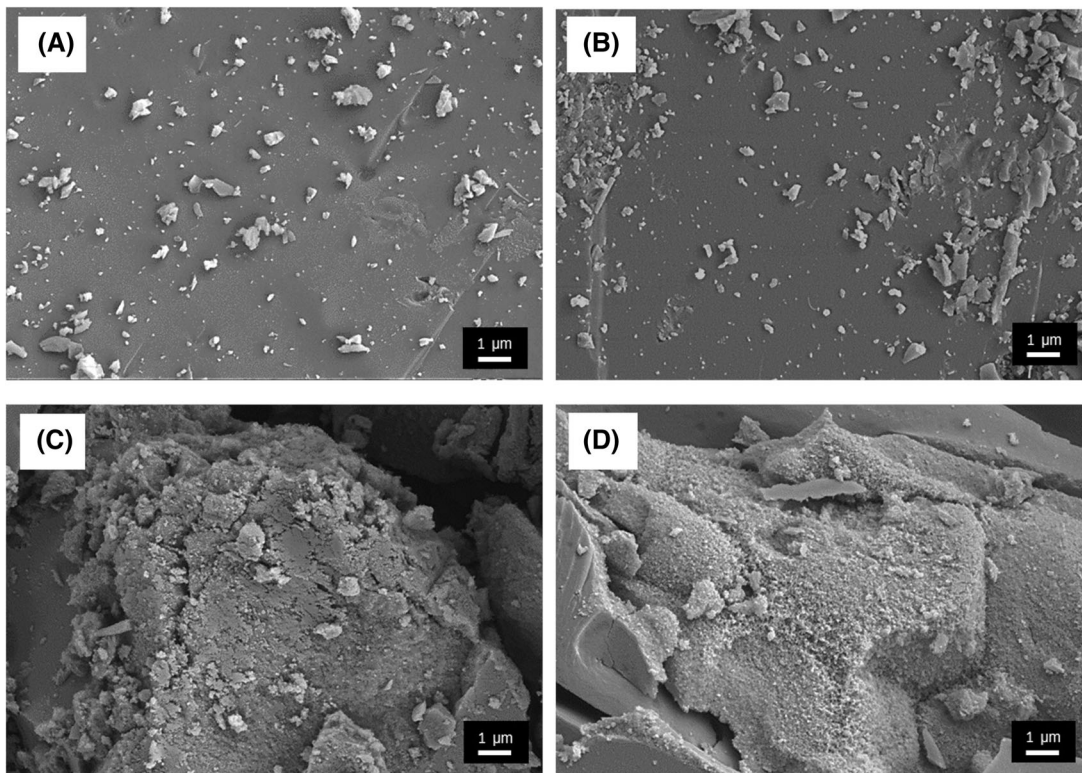


FIGURE 5 Scanning electron micrographs of (A) Si-C-N, (B) Si-Al-C-N, (C) TiN@Si-Al-C-N\_750, and (D) TiN@Si-Al-C-N\_1000 nanocomposites indicating the evolution of porosity with respect to pyrolysis temperature

30 acetylacetone was added to the aforementioned reaction  
31 mixture and pyrolyzed in nitrogen atmosphere.

32 In order to understand the bonding characteristics,  
33 the FTIR spectra of the starting precursors were taken  
34 and plotted in Figure 2 and compared. There was no  
35 noticeable difference in peaks between HTT1800 and Al  
36 modified HTT1800. However, the peaks at  $1592\text{ cm}^{-1}$   
37 (C=O stretching) and  $1531\text{ cm}^{-1}$  (C=C stretching) could  
38 be assigned to the characteristic bands of aluminum  
39 acetylacetone.<sup>29,30</sup> The peaks observed at  $3385\text{ cm}^{-1}$  (N–  
40 H stretching),  $2917\text{ cm}^{-1}$  (C–H stretching),  $2125\text{ cm}^{-1}$  (Si–H  
41 stretching),  $1260\text{ cm}^{-1}$  (C–H symmetric deformation), and  
42  $891\text{ cm}^{-1}$  (Si–N stretching) correspond to polysilazane. In  
43 the case of TiN@Si-Al-C-N precursor, the peaks observed  
44 at  $3385\text{ cm}^{-1}$  (N–H asymmetric vibrations) and  $3320\text{ cm}^{-1}$   
45 (N–H symmetric vibrations) could be assigned to urea. The  
46 peak at  $1620\text{ cm}^{-1}$  could be assigned to the presence of N–  
47 C=O bonds. The absence of Si–H peaks in the TiN@Si-Al–  
48 C–N precursor implies the complete ceramization of the  
49 Si–Al–C–N substrate at the chosen pyrolysis temperature  
50 ( $800^\circ\text{C}$ ).

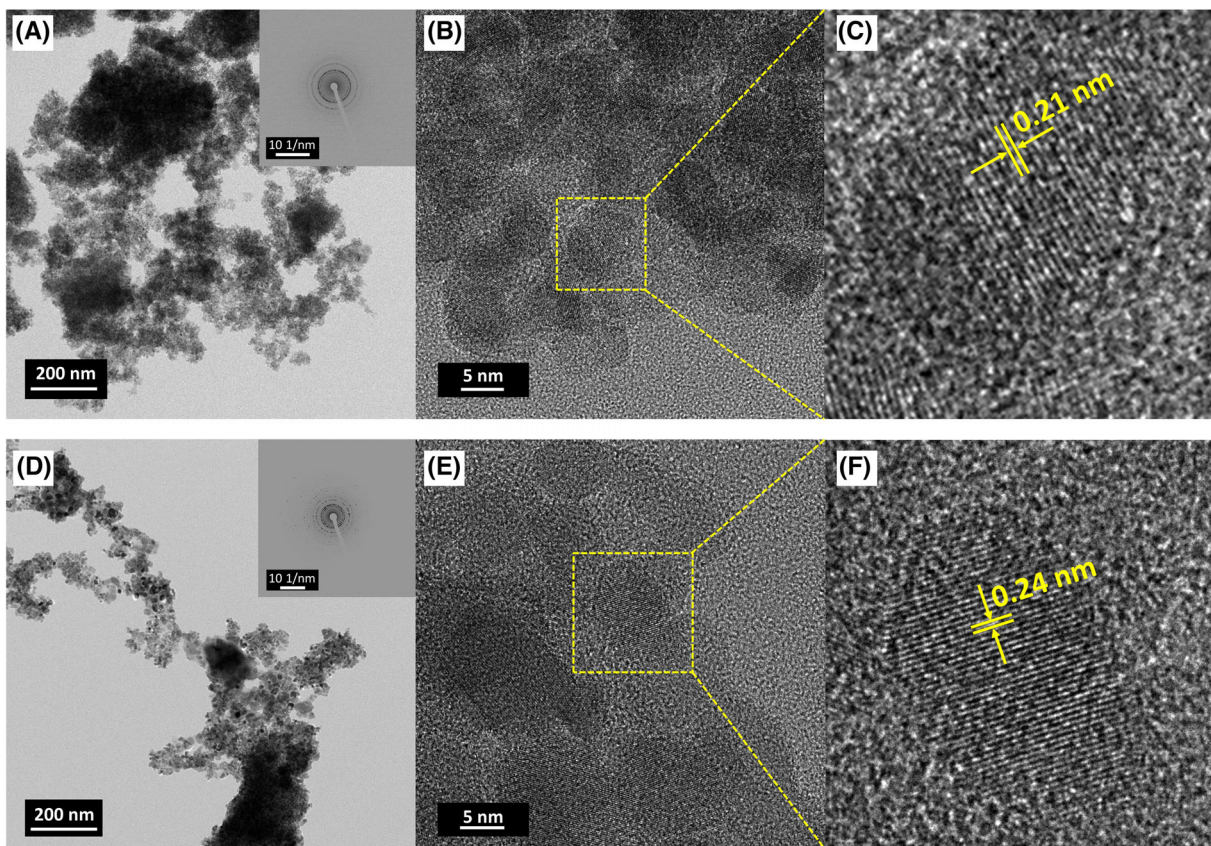
51 Raman spectroscopy was performed to analyze the  
52 presence of free carbon in the prepared ceramics. The  
53 Raman spectra clearly revealed the presence of free  
54 carbon for Si-C-N, Si-Al-C-N, TiN@Si-Al-C-N\_750,  
55 and TiN@Si-Al-C-N\_1000 nanocomposites as shown in

Figure 3 by clear D:G peaks characteristic of carbonaceous species.

The bands at  $\sim 1320$  and  $\sim 1580\text{ cm}^{-1}$  correspond to disordered carbon and in-plane vibrations of graphitic  $\text{sp}^2$  carbon, respectively. The  $I_{\text{D}}/I_{\text{G}}$  ratio (Table 1) was found to be decreasing with the modification of Si-C-N by Al and TiN (from 1.91 to .93). In the case of TiN@Si-Al-C-N\_750 and TiN@Si-Al-C-N\_1000 nanocomposites, the decrease in  $I_{\text{D}}/I_{\text{G}}$  ratio with increase in pyrolysis temperature indicates progressive graphitization.<sup>31,32</sup> This is expected to increase the electrical conductivity of the nanocomposites, thereby improving the electrocatalytic activity.<sup>33</sup>

The XRD patterns of the synthesized materials are shown in Figure 4. The Si-C-N and Si-Al-C-N ceramics were found to be amorphous in nature indicated by their featureless diffractograms. The TiN@Si-Al-C-N nanocomposites exhibited broad peaks at  $2\theta = 36.6^\circ$ ,  $42.8^\circ$ ,  $62.2^\circ$ , and  $74.4^\circ$  indicating the nanocrystalline nature of crystalline TiN. The size of the nanocrystalline TiN pyrolyzed at 750 and  $1000^\circ\text{C}$  was determined using Scherrer's formula and estimated to be 5 and 12 nm, respectively.

Figure 5 shows the SEM micrographs of the prepared catalysts. The addition of Al in the Si-C-N backbone (Figure 5B) did not cause visible changes to the microstructure of the powders. However, the introduction of TiN



**FIGURE 6** High resolution transmission electron microscopy (HRTEM) images of (A–C) TiN@Si-Al-C-N\_750 and (D–F) TiN@Si-Al-C-N\_1000 nanocomposites indicating the uniformly distributed TiN nanocrystals in the Si-Al-C-N matrix. The inset image corresponds to the SAED patterns for the synthesized nanocomposites.

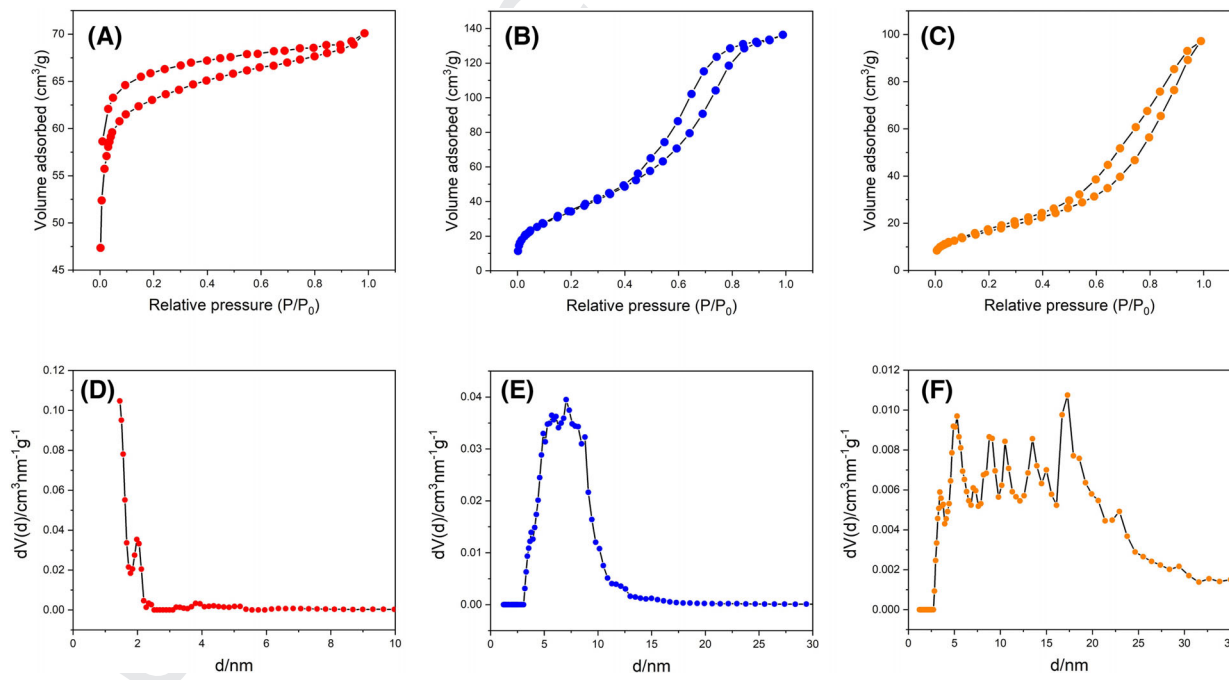


**FIGURE 7** Nitrogen adsorption–desorption isotherms and pore size distribution of (A and D) Si-Al-C-N, (B and E) TiN@Si-Al-C-N\_750, and (C and F) TiN@Si-Al-C-N\_1000 revealing the porous nature of the prepared ceramics

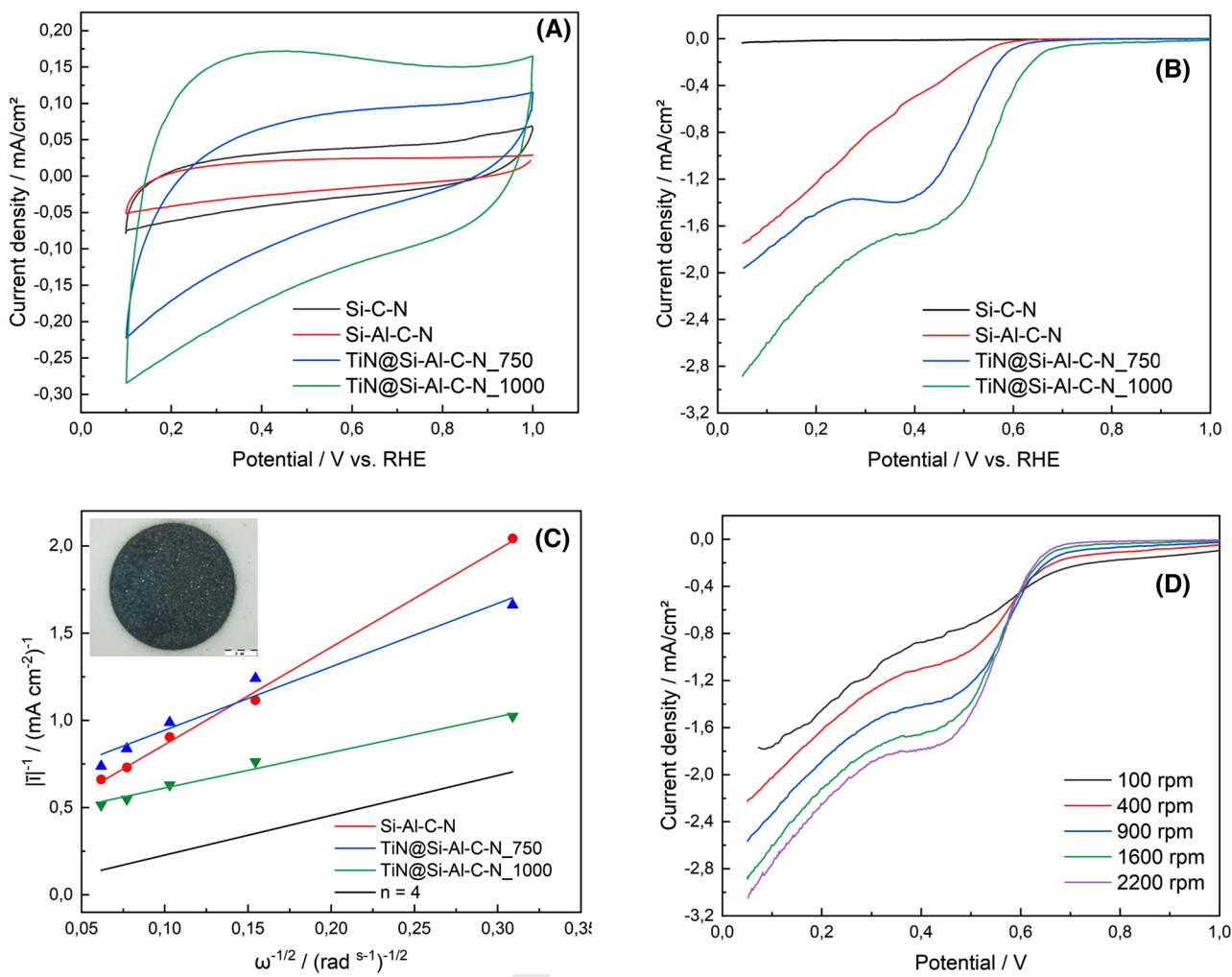


**FIGURE 8** (A) Cyclic voltammogram (CV) curves of Si-C-N, Si-Al-C-N, TiN@Si-Al-C-N\_750, and TiN@Si-Al-C-N\_1000 in N<sub>2</sub>-saturated .1 M KOH at a sweep rate of 200 mV/s (B) RDE voltammograms of Si-C-N, Si-Al-C-N, TiN@Si-Al-C-N\_750, and TiN@Si-Al-C-N\_1000 in O<sub>2</sub>-saturated .1 M KOH at 1600 rpm at a scan rate of 20 mV/s, (C) Koutecky-Levich plots of the catalyst materials at 100, 400, 900, 1600, and 2200 rpm in reference to  $n = 4$  of the exchanged number of electrons, (D) linear sweep voltammetry (LSV) scans of the TiN@Si-Al-C-N\_1000 in O<sub>2</sub>-saturated .1 M KOH at 100, 400, 900, 1600, and 2200 rpm with a scan rate of 20 mV/s

led to a change in the microstructures as shown in Figure 5C,D revealing the porous nature of the nanocomposites. The TiN@Si-Al-C-N nanocomposites exhibited TiN nanocrystals anchored on the Si-Al-C-N matrix. Moreover, the micrographs of TiN@Si-Al-C-N nanocomposites pyrolyzed at different temperatures clearly demonstrated the porous nature of the nanocomposites.

High-resolution transmission electron microscopy (HRTEM) was performed to visualize the distribution of TiN nanocrystals in the Si-Al-C-N matrix. Figure 6 shows HRTEM images of (A-C) TiN@Si-Al-C-N\_750 and (D-F) TiN@Si-Al-C-N\_1000 nanocomposites. The micrographs clearly revealed the uniform distribution of TiN nanocrystals in the Si-Al-C-N matrix. The measured crystallite size of TiN nanocrystals was in accordance with the crystallite size determined using Scherrer's formula. Figure 6C,F shows the lattice fringe spacing

of TiN@Si-Al-C-N\_750 and TiN@Si-Al-C-N\_1000 nanocomposites, respectively. The lattice fringe spacing of .21 and .24 nm corresponds to the (200) and (111) planes of TiN, respectively. The inset images in Figure 6A,D correspond to SAED patterns of TiN@Si-Al-C-N\_750 and TiN@Si-Al-C-N\_1000 nanocomposites, respectively. The discontinuous ring patterns observed in SAED further confirm the crystalline nature of the nanocomposites.

The nitrogen-desorption measurements were performed on the prepared catalysts to understand their textural characteristics and revealed surface areas as shown in Figure 7. The surface areas of Si-Al-C-N, TiN@Si-Al-C-N\_750, and TiN@Si-Al-C-N\_1000 nanocomposites were found to be 191, 132, and 58 m<sup>2</sup>/g, respectively. The Si-Al-C-N ceramics and TiN@Si-Al-C-N nanocomposites exhibited type IV isotherms with H<sub>2</sub> hysteresis loop indicating the mesoporous nature (pore

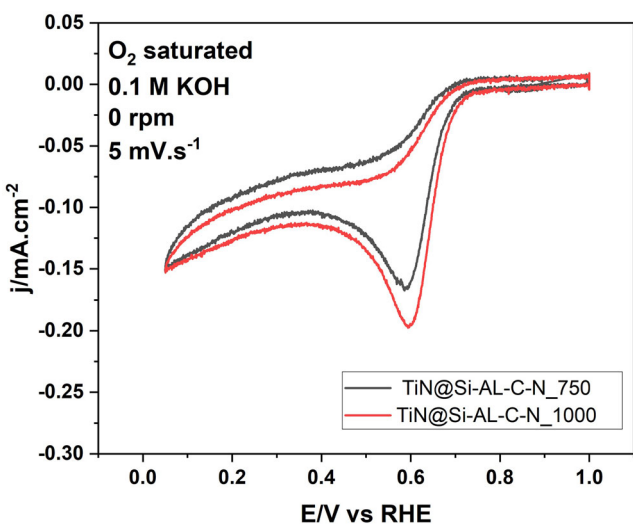


**FIGURE 9** Cyclic voltammograms (CVs) of TiN@Si-Al-C-N\_750 and TiN@Si-Al-C-N\_1000, performed in O<sub>2</sub>-saturated .1 M KOH solution with a slow scan rate of 5 mV/s (no rotation)

size in the range of 2–50 nm) of the nanocomposites. Furthermore, rather the high adsorption of nitrogen molecules at lower relative pressures  $P/P_0 < .1$  indicates the presence of micropores. It was observed that the crystallization of TiN nanocrystals on Si-Al-C-N substrate decreased the amount of adsorbed nitrogen. The average pore size was determined by DFT calculations (N<sub>2</sub> at  $-196.15^{\circ}\text{C}$  on carbon [slit pore model, NLDFT equilibrium model]), and the corresponding NLDFT pore size distributions have been shown in Figure 7D–F. The average pore sizes of Si-Al-C-N, TiN@Si-Al-C-N\_750, and TiN@Si-Al-C-N\_1000 were found to be 1.5, 7, and 17.2 nm, respectively. The average pore size of the nanocomposites was found to increase with an increase in the pyrolysis temperature.

The ORR performance of the synthesized Si-C-N, Si-Al-CN, TiN@Si-Al-C-N\_750, and TiN@Si-Al-C-N\_1000 has been thoroughly investigated and reported in Figure 8.

The CV curves in N<sub>2</sub>-saturated .1 M KOH solution are shown in Figure 8A. No specific redox peaks were observed in a potential range from .1 to 1.0 V. The curves only show non-Faradaic currents with charge and discharge of the electric double layers. Si-C-N and Si-Al-C-N supports show low double layer capacitance, whereas the non-Faradaic current of the TiN-based catalysts increases with the pyrolysis temperature. This might be caused by the amount of carbon in the support material, which depends on the pyrolysis temperature and also affects the electrical conductivity. Figure 8B shows the ORR activity measured by the LSV polarization curve of the Si-Al-C-N and TiN@Si-Al-C-N (pyrolyzed at 750 and 1000°C) catalysts at a sweep rate of 20 mV/s and a rotation speed of 1600 rpm.

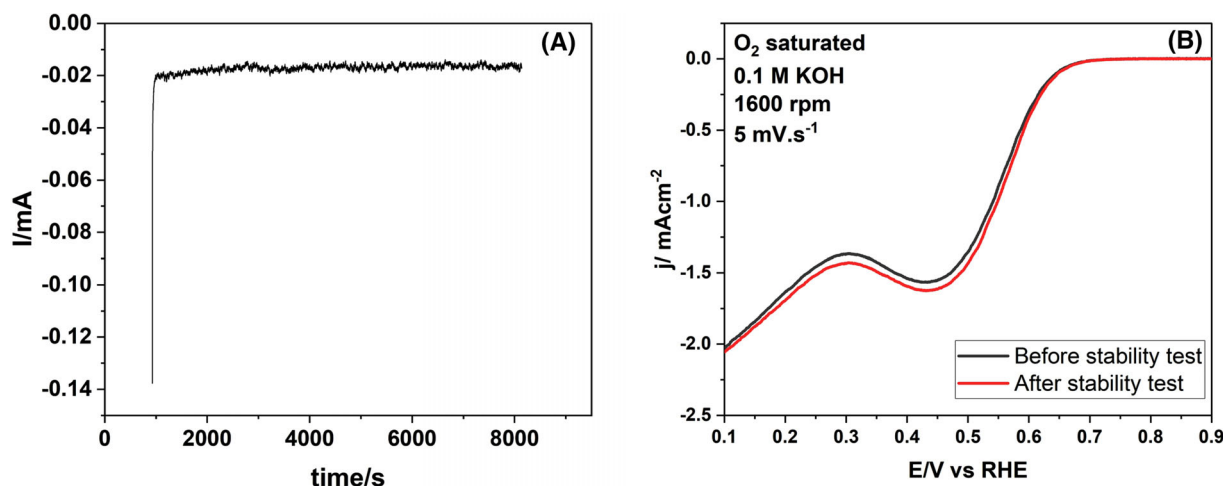
It can be seen that the different samples exhibit significantly different current densities. Although the Si-C-N support does not contribute to ORR, the activity increases to about 1.7 mA/cm<sup>2</sup> when Al is added into the sample. Higher ORR activities are measured for the pyrolyzed TiN samples. The carbon content varies with pyrolysis temperature and therefore has a significant effect on the limiting current density and onset potential. The current densities for Si-C-N, Si-Al-C-N, TiN@Si-Al-C-N\_750, and TiN@Si-Al-C-N\_1000 at .58 V are .006, .04, .15, and .6 mA/cm<sup>2</sup>, respectively. The corresponding plots for the Koutecky-Levich (K-L) analysis are shown in Figure 8C. K-L plots allow us to evaluate the first-order reaction, knowing the amount of dissolved oxygen in the electrolyte and the calculation of the electron transfer number per oxygen molecule during ORR. Figure 8D shows the LSV curves for TiN@Si-Al-C-N\_1000 at various rotating speeds. The number of transferred electrons for Si-C-N, Si-Al-C-N, TiN@Si-Al-C-N\_750, and TiN@Si-Al-C-N\_1000 in a potential range from .35 to .55 V was calculated as .008, 1.63, 2.23, and 3.85 electrons, in comparison to the desired 4e<sup>-</sup> process, which is obtained during the catalysis of ORR by the noble metal Pt.

The CVs of TiN@Si-Al-C-N\_750 and TiN@Si-Al-C-N\_1000 were also performed at a slow scan rate of 5 mV/s in O<sub>2</sub>-saturated .1 M KOH solution with no rotation. A similar correlation between TiN@Si-Al-C-N\_750 and TiN@Si-Al-C-N\_1000 was observed as shown in Figure 9.

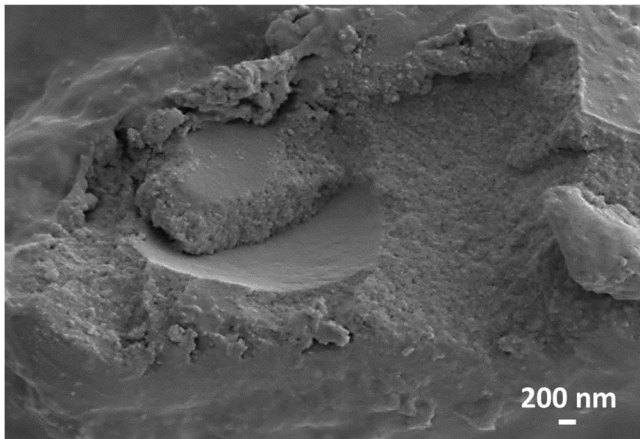
The reported onset potential of TiN-based catalysts was between .5 and .83 V. For instance, .6 V has been reported for bulk TiN,<sup>20</sup> .85 V for TiN hollow spheres,<sup>34</sup> .83 V for TiN/graphene-CNT,<sup>20</sup> and .5 V for TiON@nitrogen-doped carbon spheres.<sup>9</sup> In this study, the onset potential of TiN@Si-Al-C-N\_1000 was found to be .7 V.

In order to understand the stability of the catalyst, CA was performed on TiN@Si-Al-C-N\_1000 at the potential of .6 V for 2 h (Figure 10A), where we observed significant activity in the ORR curve. After a hold time at OCV for 15 min, the current stabilized at around  $-.02$  mA and was stable for the whole duration of the CA. The CVs (anodic scans) of TiN@Si-Al-C-N\_1000, in O<sub>2</sub>-saturated .1 M KOH solution with a slow scan rate of 5 mV/s and a rotation rate of 1600 rpm, are reported in Figure 10B before and after the stability test. It can be seen that a slight increase in the catalytic activity was observed after the CA treatment.

SEM images of the TiN@Si-Al-C-N\_1000 nanocomposites were obtained after the ORR test, and an exemplary micrograph is shown in Figure 11. There was no significant change observed in the microstructure (apart from a slight decrease in the porosity) post ORR test implying the stability during the test time frame of the prepared nanocomposites. However, it needs to be considered that the testing time was comparatively low. Furthermore, as



18 **FIGURE 10** (A) Stability test (chrono-amperometric [CA]) of TiN@Si-Al-C-N\_1000 performed in O<sub>2</sub>-saturated .1 M KOH at .6 V for  
19 2 h. (B) cyclic voltammograms (CVs) (anodic scan) of TiN@Si-Al-C-N\_1000, performed in O<sub>2</sub>-saturated .1 M KOH solution with a slow scan  
20 rate of 5 mV/s (1600 rotation)



36 **FIGURE 11** Scanning electron micrograph of  
37 TiN@Si-Al-C-N\_1000 nanocomposites after oxygen reduction  
38 reaction (ORR) test

40 the catalyst film on the RDE is very thin, not enough  
41 post material could be collected for further testing by BET,  
42 Raman, and XRD.

## 4 | CONCLUSIONS

47 TiN@Si-Al-C-N nanocomposites were prepared using a  
48 combination of PDC approach with urea-glass route. The  
49 synthesized nanocomposites were explored for their elec-  
50 trocatalytic (ORR) properties in alkaline media using RDE.  
51 The XRD diffractograms revealed the crystallization of TiN  
52 in an amorphous Si-Al-C-N matrix with sizes ranging  
53 from 5 to 12 nm. The SEM micrographs also confirmed the  
54 anchoring of TiN nanocrystals on an Si-Al-C-N substrate.  
55 The prepared TiN@Si-Al-C-N nanocomposites possessed

a surface area of 132 and 58 m<sup>2</sup>/g at 750 and 1000°C, respec-  
tively, and were found to be mesoporous in nature. The  
presence of TiN on the silicon-based ceramics was found  
to trigger an ORR response in alkaline media. Si-C-N, Si-  
Al-C-N, and TiN@Si-Al-C-N\_750 led to a two-electron  
pathway with H<sub>2</sub>O<sub>2</sub> formation in ORR, whereas TiN@Si-  
Al-C-N\_1000 led to a four-electron pathway for the ORR  
in alkaline media. In the future, other electrocatalytically  
active centers, such as Fe that is also low-cost, non-  
toxic, and earth-abundant, could be implemented into  
these promising N-containing support materials, further  
increasing activity without the compromising stability of  
the materials.

## ACKNOWLEDGMENTS

The authors would like to thank the Deutsche Forschungs-  
gemeinschaft (DFG) and the Agence Nationale de la  
Recherche (ANR) for funding the work through the  
RECIFE project (Project Numbers: DFG MO851/22-1 and  
ANR-21-CE08-0036-01).

## ORCID

Timon E. Günther <https://orcid.org/0000-0002-3678-0999>

Stefan Schafföner <https://orcid.org/0000-0002-6526-2496>

Günter Motz <https://orcid.org/0000-0002-8010-068X>

## REFERENCES

1. Shimizu K, Sepunaru L, Compton RG. Innovative catalyst design for the oxygen reduction reaction for fuel cells. *Chem Sci*. 2016;7(5):3364–9.
2. Lori O, Elbaz L. Advances in ceramic supports for polymer electrolyte fuel cells. *Catalysts*. 2015;5(3):1445–64.

3. Shao M, Chang Q, Dodelet JP, Chenitz R. Recent Advances  
4. in electrocatalysts for oxygen reduction reaction. *Chem Rev.*  
5. 2016;116:3594–657.

6. Chung HT, Cullen DA, Higgins D, Sneed BT, Holby EF,  
7. More KL, et al. Direct atomic-level insight into the active  
8. sites of a high-performance PGM-free ORR catalyst. *Science.*  
9. 2017;357(6350):479–84. Available from: <https://www.science.org>

10. Guo D, Shibuya R, Akiba C, Saji S, Kondo T, Nakamura  
11. J. Active sites of nitrogen-doped carbon materials for oxy-  
12. gen reduction reaction clarified using model catalysts. *Science.*  
13. 2016;351(6271):361–5. Available from: <https://www.science.org>

14. Dong Y, Wu Y, Liu M, Li J. Electrocatalysis on shape-controlled  
15. titanium nitride nanocrystals for the oxygen reduction reaction.  
16. *ChemSusChem.* 2013;6(10):2016–21.

17. Yuan Y, Wang J, Adimi S, Shen H, Thomas T, Ma R, et al. Zir-  
18. conium nitride catalysts surpass platinum for oxygen reduction.  
19. *Nat Mater.* 2020;19:280–6.

20. Zheng S, Luo R, Meng Z, Wang R, Tan H, Xia Y, et al. Recent  
21. advances in the electrocatalytic application of transition metal  
22. nitrides nanocrystalline. 2021. Available from: [www.preprints.org](https://www.preprints.org)

23. Wassner M, Eckardt M, Reyer A, Diemant T, Elsaesser MS,  
24. Behm RJ, et al. Synthesis of amorphous and graphitized porous  
25. nitrogen-doped carbon spheres as oxygen reduction reaction  
26. catalysts. *Beilstein J Nanotechnol.* 2020;11:1–15.

27. Wang H, Keum JK, Hiltner A, Baer E, Freeman B, Rozanski A,  
28. et al. Confined crystallization of polyethylene oxide in nanolayer  
29. assemblies. *Science (80–).* 2009;323(5915):757–60.

30. Zhang L, Xia Z. Mechanisms of oxygen reduction reaction  
31. on nitrogen-doped graphene for fuel cells. *J Phys Chem C.*  
32. 2011;115(22):11170–6.

33. Lv Q, Si W, He J, Sun L, Zhang C, Wang N, et al. Selectively  
34. nitrogen-doped carbon materials as superior metal-free catalysts  
35. for oxygen reduction. *Nat Commun.* 2018;9(1).

36. Su F, Tian Z, Poh CK, Wang Z, Lim SH, Liu Z, et al. Pt nanopar-  
37. ticles supported on nitrogen-doped porous carbon nanospheres  
38. as an electrocatalyst for fuel cells. *Chem Mater.* 2010;22(3):  
39. 832–9.

40. Li M, Xu F, Li H, Wang Y. Nitrogen-doped porous carbon mate-  
41. rials: promising catalysts or catalyst supports for heterogeneous  
42. hydrogenation and oxidation. *Catal Sci Technol.* 2016;6:3670–  
43. 93.

44. Zheng Y, He F, Wu J, Ma D, Fan H, Zhu S, et al. Nitrogen-  
45. doped carbon nanotube-graphene frameworks with encapsu-  
46. lated Fe/Fe<sub>3</sub>N nanoparticles as catalysts for oxygen reduction.  
47. *ACS Appl Nano Mater.* 2019;2(6):3538–47.

48. Shi Q, Zhu C, Engelhard MH, Du D, Lin Y. Highly uniform dis-  
49. tribution of Pt nanoparticles on N-doped hollow carbon spheres  
50. with enhanced durability for oxygen reduction reaction. *RSC  
51. Adv.* 2017;7(11):6303–8.

52. Bokach D, ten Hoopen S, Muthuswamy N, Buan MEM,  
53. Rønning M. Nitrogen-doped carbon nanofiber catalyst for ORR  
54. in PEM fuel cell stack: performance, durability and market  
55. application aspects. *Int J Hydrogen Energy.* 2016;41(39):17616–  
30.

18. Sarkar S, Kamboj N, Das M, Purkait T, Biswas A, Dey RS. Uni-  
versal approach for electronically tuned transition-metal-doped  
graphitic carbon nitride as a conductive electrode material  
for highly efficient oxygen reduction reaction. *Inorg Chem.*  
2020;59(2):1332–9.

19. Liu Z, Fu X, Li M, Wang F, Wang Q, Kang G, et al. Novel silicon-doped, silicon and nitrogen-codoped carbon nano-  
materials with high activity for the oxygen reduction reac-  
tion in alkaline medium. *J Mater Chem A.* 2015;3(7):3289–  
93.

20. Youn DH, Bae G, Han S, Kim JY, Jang JW, Park H, et al. A highly  
efficient transition metal nitride-based electrocatalyst for oxy-  
gen reduction reaction: TiN on a CNT-graphene hybrid support.  
*J Mater Chem A.* 2013;1(27):8007–15.

21. Zeng R, Yang Y, Feng X, Li H, Gibbs LM, Disalvo FJ, et al. Non-  
precious transition metal nitrides as efficient oxygen reduction  
electrocatalysts for alkaline fuel cells. *Sci Adv.* 2022;8:eabj1584.  
Available from: <https://www.science.org>

22. Borup R, Meyers J, Pivovar B, Kim YS, Mukundan R, Garland N,  
et al. Scientific aspects of polymer electrolyte fuel cell durability  
and degradation. *Chem Rev.* 2007;107:3904–51.

23. McCreery RL. Advanced carbon electrode materials for molec-  
ular electrochemistry. *Chem Rev.* 2008;108:2646–87.

24. Colombo P, Mera G, Riedel R, Soraru GD. Polymer-derived  
ceramics: 40 years of research and innovation in advanced  
ceramics. *J Am Ceram Soc.* 2010;93(7):1805–37. Available from:  
<http://doi.wiley.com/10.1111/j.1551-2916.2010.03876.x>

25. Mera G, Gallei M, Bernard S, Ionescu E. Ceramic nanocom-  
posites from tailor-made preceramic polymers. *Nanomaterials.*  
2015;5:468–540.

26. Awin EW, Lale A, Nair Hari Kumar KC, Demirci UB, Bernard  
S, Kumar R. Novel precursor-derived meso-/macroporous  
TiO<sub>2</sub>/SiOC nanocomposites with highly stable anatase  
nanophase providing visible light photocatalytic activity  
and superior adsorption of organic dyes. *Materials (Basel).*  
2018;11(3):362.

27. Viard A, Kurz H, Lale A, Heymann L, Weber B, Bernard S, et al.  
Superparamagnetic silicon carbonitride ceramic fibers through  
in situ generation of iron silicide nanoparticles during pyroly-  
sis of an iron-modified polysilazane. *ACS Appl Mater Interfaces.*  
2021;13(7):8745–53.

28. David L, Asok D, Singh G. Synthesis and extreme rate capa-  
bility of Si-Al-C-N functionalized carbon nanotube spray-on  
coatings as li-ion battery electrode. *ACS Appl Mater Interfaces.*  
2014;6(18):16056–64.

29. Soraru GD, Mercadini M, Maschio RD, Taulelle F, Babonneau  
F. Si-Al-O-N fibers from polymeric precursor: synthesis, struc-  
tural and mechanical characterization. *J Am Ceram Soc.*  
1993;76(10):2595–600.

30. Yang L, Zhang P, Feng Y, Yu Z. Single-source-precursor syn-  
thesis and characterization of SiAlC(O) ceramics from a hyper-  
branched polyaluminocarbosilane. *High Temp Mater Processes.*  
2022;41:150–60.

31. Mera G, Riedel R, Poli F, Müller K. Carbon-rich SiCN ceramics  
derived from phenyl-containing poly(silylcarbodiimides). *J Eur  
Ceram Soc.* 2009;29(13):2873–83.

32. Gao Y, Mera G, Nguyen H, Morita K, Kleebe HJ, Riedel R.  
Processing route dramatically influencing the nanostructure of  
carbon-rich SiCN and SiBCN polymer-derived ceramics. Part  
I: Low temperature thermal transformation. *J Eur Ceram Soc.*  
2012;32(9):1857–66.

3 33. Feng Y, Yu Z, Riedel R. Enhanced hydrogen evolution reaction  
4 catalyzed by carbon-rich Mo4.8Si3C0.6/C/SiC nanocomposites  
5 via a PDC approach. *J Am Ceram Soc.* 2020;103(2):1385–  
6 95.

7 34. Chen J, Wei X, Zhang J, Luo Y, Chen Y, Wang G, et al. Titanium  
8 nitride hollow spheres consisting of tin nanosheets and  
9 their controllable carbon-nitrogen active sites as efficient elec-  
10 trocatalyst for oxygen reduction reaction. *Ind Eng Chem Res.*  
11 2019;58(8):2741–8.

12

13

14

15

16

17

18

19

20

21

22

23

24

25

26

27

28

29

30

31

32

33

34

35

36

37

38

39

40

41

42

43

44

45

46

47

48

49

50

51

52

53

54

55

**How to cite this article:** Awin EW, Günther TE, Loukrakpam R, Schafföner S, Roth C, Motz G. Synthesis and characterization of precursor derived TiN@Si-Al-C-N ceramic nanocomposites for oxygen reduction reaction. *Int J Appl Ceram Technol.* 2022;1–11. <https://doi.org/10.1111/ijac.14234>